The effect of skin thickness determined using breast CT on mammographic dosimetry

Shih-Ying Huang, John M. Boone,[a] and Kai Yang
Department of Biomedical Engineering, University of California, One Shields Avenue, Davis, California 95616 and Department of Radiology, X-Ray Imaging Laboratory, U.C. Davis Medical Center, 4701 X Street, Sacramento, California 95817

Alexander L. C. Kwan
Department of Radiology and Diagnostic Imaging, Division of Imaging Sciences, Research Transition Facility, University of Alberta, 8308-114 Street, Room 4105, Edmonton, Alberta T6G 2E1, Canada

Nathan J. Packard
Department of Biomedical Engineering, University of California, One Shields Avenue, Davis, California 95616 and Department of Radiology, X-Ray Imaging Laboratory, U.C. Davis Medical Center, 4701 X Street, Sacramento, California 95817

(Received 24 October 2007; revised 15 January 2008; accepted for publication 17 January 2008; published 6 March 2008)

The effect of breast skin thickness on dosimetry in mammography was investigated. Breast computed tomography (CT) acquisition techniques, combined with algorithms designed for determining specific breast metrics, were useful for estimating skin thickness. A radial-geometry edge detection scheme was implemented on coronal reconstructed breast CT (bCT) images to measure the breast skin thickness. Skin thickness of bilateral bCT volume data from 49 women and unilateral bCT volume data from 2 women (10 healthy women and 41 women with BIRADS 4 and 5 diagnoses) was robustly measured with the edge detection scheme. The mean breast skin thickness ($\pm$inter-breast standard deviation) was found to be 1.45 ± 0.30 mm. Since most current published normalized glandular dose (D_{gN}) coefficients are based on the assumption of a 4-mm breast skin thickness, the D_{gN} values computed with Monte Carlo techniques will increase up to 18% due to the thinner skin layers (e.g., 6-cm 50% glandular breast, 28 kVp Mo–Mo spectrum). The thinner skin dimensions found in this study suggest that the current D_{gN} values used for mammographic dosimetry lead to a slight underestimate in glandular dose. © *2008 American Association of Physicists in Medicine*. [DOI: 10.1118/1.2841938]

Key words: edge detection, breast skin thickness, breast CT, normalized glandular dose coefficients

I. INTRODUCTION

Dosimetry for both screen-film and digital mammography relies directly on the normalized glandular dose (D_{gN}) coefficients which are determined using Monte Carlo computations.[1,2] For most D_{gN} coefficients that are used in the United Kingdom and the United States, the skin thickness surrounding the breast was assumed to be 4 mm.[3–8] While skin thickness is a relatively minor consideration in breast dosimetry in regards to mammography, the skin surrounding the breast tissue does act much like an x-ray beam filter, preferentially removing low-energy x-ray photons which contribute primarily to radiation dose to the breast. In addition to the slight beam filtration effect, the skin layer on the x-ray entrant side of the breast experiences the full incident x-ray beam, and tissues at greater depth receive exponentially less of the x-ray beam intensity.

Recent investigations in our laboratory have focused on the engineering development and clinical implementation of breast computed tomography (CT).[9] Access to the high-resolution breast CT (bCT) images from 51 women has allowed the assessment of skin thickness for the screening population. Based upon the observation of these images, and because the skin thickness is known to play at least a minor role in breast dosimetry, an analysis of the skin thickness on bCT images was performed to develop a more accurate understanding of the range of skin thickness encountered in the clinical screening population.

II. METHODS AND MATERIALS

II.A. Patient population

A prototype breast CT scanner was used to conduct phase I and II clinical trial studies under several IRB-approved protocols. In the phase I trial, breast CT images were acquired from 10 healthy women volunteers. During phase II testing, women who may have breast cancer (BIRADS 4 and 5) were imaged in order to evaluate the efficacy of breast CT for the early detection of breast cancer. BCT images were acquired prior to the breast biopsy. A total of 100 single breast volume data sets from 51 women were used to analyze the breast skin thickness (bilateral bCT volume sets from 49 women; unilateral bCT volume data from 2 women). Fifty-eight breast volume sets were the healthy breasts of normal volunteers and the contralateral breasts of those with benign findings and breast cancer. Two breast volume sets were the breasts with benign findings, while the remaining 40 breast

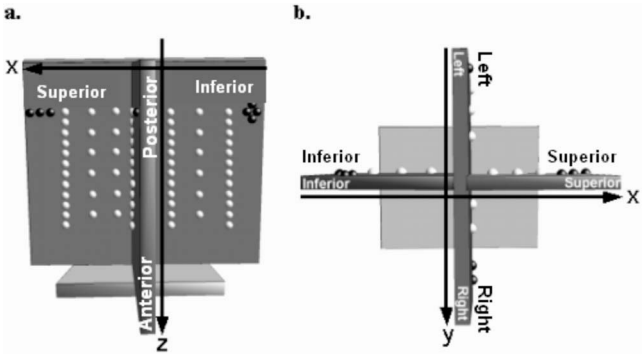

FIG. 1. The spatial accuracy phantom was constructed with two foam boards, as shown in the (a) side view and (b) top view. The corresponding *x*, *y*, and *z* dimensions in a reconstructed volume set are illustrated as well.

volume sets were diagnosed with breast cancer. The bra cup size was used as a parameter in x-ray technique selection, and the 51 women examined in this investigation had the following distribution: A cup: 1, B: 12, C: 20, D: 14, and DD: 4.

II.B. Breast CT scanner

A dedicated breast CT scanner (dubbed "Albion") was designed, fabricated under contract by a local machine shop, assembled, and integrated in our laboratory.[9] This scanner was used to acquire the bCT images used in this investigation. The breast CT scanner operates at 80 kVp, and the technique factors (mA s) were selected based on the self-reported bra cup size of the patient. The mA s was selected such that the mean glandular dose from the bCT scan was virtually identical to two-view mammography for each woman.[9] The CT scan was performed in the coronal plane, imaging only a single breast in pendant geometry with the woman prone on the scanner tabletop with the breast hanging through a circular hole in the table. The x-ray tube and the detector system rotate around the pendant breast in the horizontal plane. The current cone-beam CT reconstruction generates bCT images in Hounsfield units and it also corrects for beam hardening and scatter using a numerical normalization method.[10] The cone-beam CT reconstruction typically produces 200–512 breast CT images per breast. The 512×512 reconstructed CT images have pixel dimensions ranging between 194 and 407 μm (depending on the size of the breast) and slice thickness is approximately 0.21 mm. The *x*, *y*, and *z* voxel dimensions and the slice position information in the vertical plane are embedded in the custom header of the bCT images.

II.C. Image evaluation

II.C.1. Spatial accuracy

To ensure the accuracy of the skin thickness analysis, the measured and actual voxel positions in the *x*, *y*, and *z* directions from a reference phantom were compared. A phantom was designed and constructed as shown in Fig. 1. It was composed of two foam boards crossed and secured on a platform. On each board, a number of 6-mm, round, plastic pellets (BBs) were securely placed in several columns that were 25 mm apart. Six or more BBs were placed 1.0 or 2.0 cm apart in each column. The true physical distance between the BBs in *x* and *y* direction was measured with a standard ruler. The orientation of the boards was designed such that distances between BBs in the *x* and *y* plane could be directly measured from the reconstructed images in the coronal view. Distances in the *z* direction were determined by examining the slice position (*z*) embedded in the header of the reconstructed images. The true distance between the BBs in the image data sets along the *z* direction was independently computed using custom software.[11] This software individually tracked the projection position of all BBs relative to the detector plane in one column from 500 acquired projection images to compute the true physical distance between each BB in the *z* direction. CT scan data sets were acquired in order to precisely locate columns of steel BBs at 11 different positions. Linear regression was used to fit the distances determined from the images against the physically measured distances. The orientation of the reconstructed bCT images was also verified from the design of this phantom, as the top corners of the foam boards were labeled with different numbers of BBs representing the four orientations within a bCT image. The correct orientation of the reconstructed bCT images, however, was not crucial in this analysis.

II.C.2. Skin thickness assessment

The image data sets of 51 women (100 breasts) were downloaded to a workstation, and breast skin thickness was evaluated. For the coronal bCT images, the breast silhouette was segmented from the air surround using a threshold value computed by a histogram-based iterative algorithm.[12] The iterative algorithm computed an optimal threshold by recursively searching for the best image intensity which distinguishes between the breast tissue and background (air) gray scale. The image histogram was separated into two regions based on the average of the gray scale values within two user-defined regions. With this approach, the portion of bCT image corresponding to air was suppressed to a gray scale value of zero.

Segmentation of the breast skin layer was implemented with a simple derivative filter in a circular-ray tracing fashion. Skin segmentation was performed on the coronal images. The center of mass was determined for the breast in each image. From the center of mass, a line was projected outward at 0.5-deg intervals for a 360-deg radial evaluation of the image [Fig. 2(a)]. Each line continued to the edge of the breast, or one pixel inward from where the surrounding air was previously segmented. In order to rectify any under or over estimation of skin exterior, the Euclidean distance between the center of mass and the skin edge (skin exterior length) was evaluated. The skin exterior length as a function of angle was replaced with the mean skin exterior length (determined over 360 deg) of the adjacent skin exteriors if it significantly deviated from the mean skin exterior length. This procedure had the effect of smoothing the skin contour.

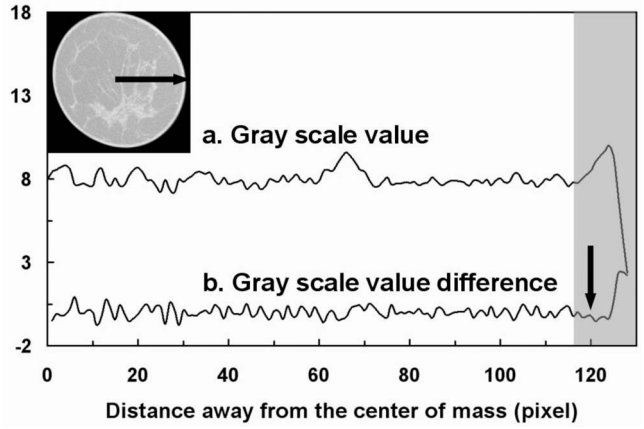

FIG. 2. (a) A profile acquired from the 360-deg radial scan illustrating the gray value distribution of a breast from the center of mass toward the skin edge for the 0-deg profile. (b) This curve illustrates the gray value difference determined by applying a first-order derivative filter to the profile in (a). The gray region designates the region of interest in locating the inner skin layer.

Each profile was evaluated from the breast edge inward, in the direction toward the center of mass. To account for the ambiguity between glandular tissue and skin (which have very similar gray scale values), the search range was restricted to 5 mm. Based on simulations and performance on the bCT images, it was found that this resulted in robust detection of the inner skin layer. The actual number of pixels evaluated in this process varied, since each breast volume set had slightly different pixel dimensions. A first-order derivative filter was applied along each profile to differentiate the gray-level intensity between a pixel and its outward adjacent pixel. The inner skin layer was positioned one pixel inward (toward the center of mass) from the pixel transition having the minimum gradient [Fig. 2(b)].

The position of the inner and outer skin layers located by the preliminary radial evaluation did not reflect the best estimate of the border locations due to the presence of noise. With the 720 locations of inner and outer skin layers initially determined at 0.5-deg increments around the breast, the Euclidean distance between the inner and outer skin layer positions was computed as the preliminary skin thickness, as a function of angle. The computed thickness was spatially filtered with a 1×5 average kernel to reduce the level of noise in the preliminary skin thickness evaluation. The average kernel used is defined in Eq. (1),

$$g(x) = \sum_{k=1}^{M} s(x+k)h(k),$$

$$h(x) = \frac{1}{M}, \quad x = -\frac{M}{2}, \ldots, \left(\frac{M}{2} - 1\right), \tag{1}$$

where $s(x)$ is the nonsmoothed skin thickness, $h(x)$ is the average kernel of size M, and $g(x)$ is the smoothed skin thickness. The noise-reduced, finely sampled inner and outer breast skin boundaries were determined for each bCT coronal image (at a specific position along the breast anterior-posterior direction). The collection of inner and outer two-dimensional skin boundaries for all of the coronal bCT images represented a three-dimensional (3D) description of the breast boundaries, i.e., a set of 3D point clouds. The 3D breast boundaries were used to determine the actual skin thickness, taking into consideration the curvature of the breast in the anterior-posterior direction (this procedure is described in the next paragraph).

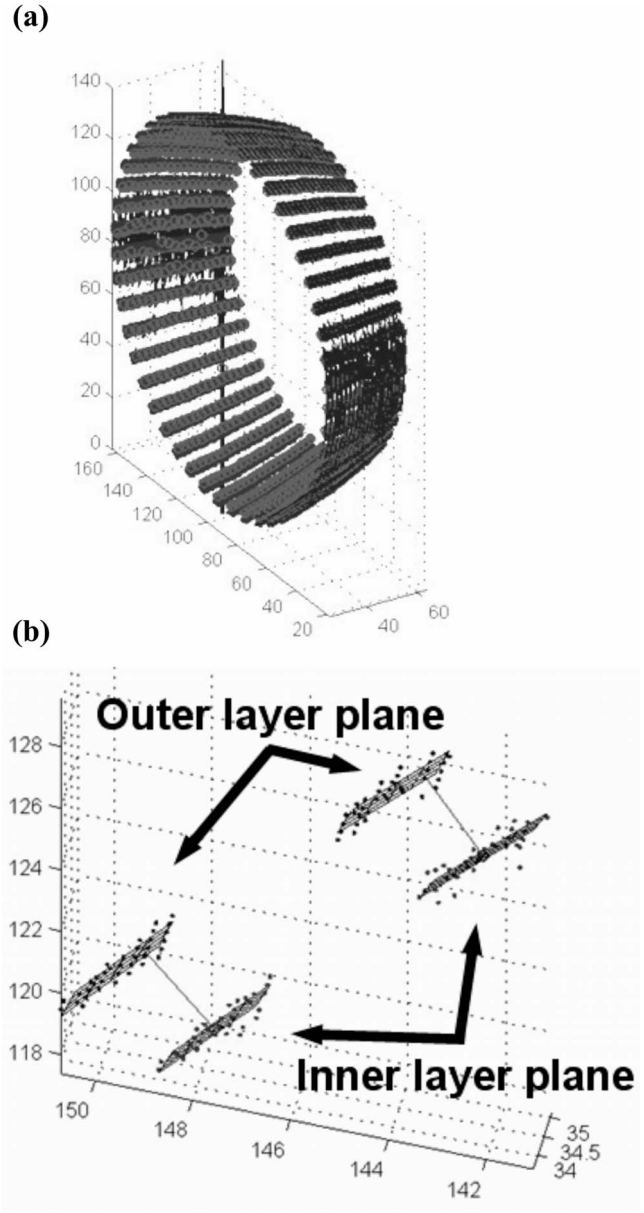

FIG. 3. The three-dimensional, patch-by-patch plane-fitting method to measure the breast skin thickness is illustrated. The fitted planes of the inner and outer wall layers are shown from the CT images of the physical phantom. (a) This graph illustrates the three-dimensional planes (least-square fitted) to the inner and outer layers over the entire surface. (b) The thickness was measured with the distance originating from a point on the fitted inner layer plane along its normal to the outer layer plane.

The most accurate estimate of breast skin thickness was to measure the distance between the inner and outer skin layers with respect to the 3D normal to the surface of the breast. To

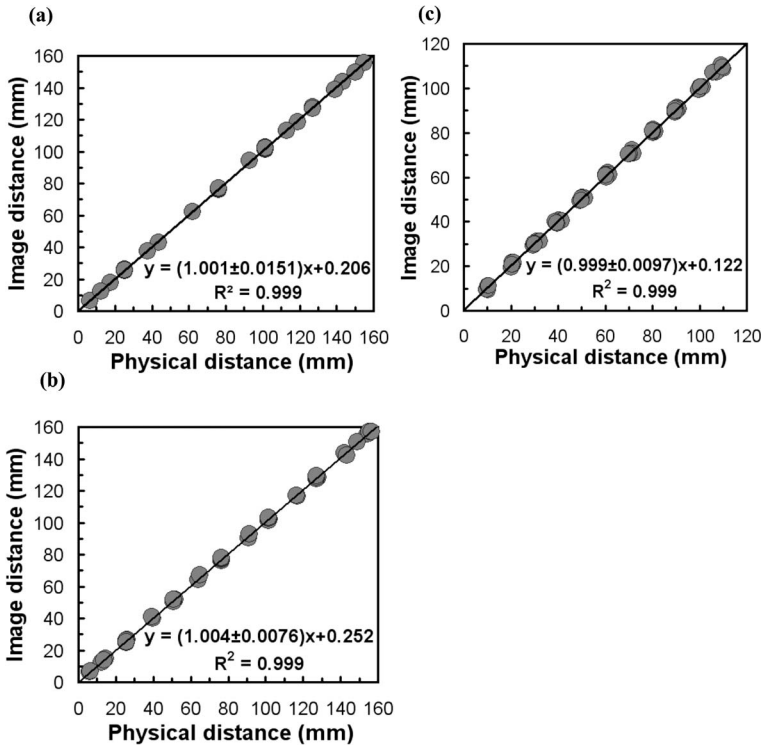

FIG. 4. The relative physical distances are shown for the (a) x, (b) y, and (c) z dimension of a reconstructed volume as a function of the relative distances measured from the reconstructed image.

realistically fit the 3D surface, a set of small surface patches which spanned the breast surface in 3D was used [Fig. 3(a)]. At a radial location of a specific z position, 36 surrounding sampled points were used to fit a plane in a least-square fashion (using an opened source plane fitting routine[13]). Two planes corresponding to the inner and outer skin layers were fit to the surface patches. The breast skin thickness was measured by determining the distance from the 3D normal of the inner skin plane to the outer skin plane [Fig. 3(b)]. Forty-eight radial locations were used at each z position (the number of z positions depends on the breast length) to determine the skin thickness of a given breast. To eliminate obvious outliers among the skin thickness estimate from the least-square approach, the 10% trimmed mean among the skin thickness estimate across the fitted breast surface was computed as the single "skin thickness" for each breast. The mean, standard deviation, and range of the measured skin thickness were evaluated for 100 breasts corresponding to 51 women. In addition, distributions of the skin thickness estimate among different breast metrics (bra cup size A, B, C, D, and DD; right versus left breast) were determined.

II.C.3. Algorithm validation

In order to validate the accuracy of the skin-thickness algorithm, a physical phantom was constructed using a water-filled plastic bowl. A CT scan of the bowl was acquired using the breast CT scanner. The wall thickness around the bowl was physically measured with a micrometer (Starrett N. 436–1IN, 0.001-in. precision) at several locations around the surface of the bowl. The average value among the wall thickness of the physical phantom was considered as "truth" to compare with the algorithmically determined wall thickness of the corresponding portion of the physical phantom. The histogram of the estimated wall thickness of the physical phantom was evaluated to examine the accuracy of the thickness measurements.

II.D. Breast dosimetry in mammography with Monte Carlo simulation

Previously validated Monte Carlo techniques[1,2,8] were used to assess the normalized glandular dose coefficients (D_{gN}) in mammography over a range of breast thickness (2–8 cm), x-ray energies (4–35 keV), and skin thickness (1.0–4.0 mm). The simulation was implemented based on the x-ray spectrum with molybdenum anode-molybdenum filter (Mo–Mo).[8] D_{gN} values were determined using one million photons in a monoenergetic simulation and a spectral model was used to convert the monoenergetic data to the polyenergetic D_{gN} values.[8]

III. RESULTS

III.A. Spatial accuracy

Figures 4(a)–4(c) show the relationship between distances measured using the bCT image data as a function of physical measurements, for the x, y, and z dimensions, respectively. Each of these curves is seen to lie very close to the line of identity. Linear regression was also used and the best-fit lines fall closely to the slope (1.0) and intercept (0.0) of the line of identity, with some bias at small values.

III.B. Algorithm validation

Among 61 manual thickness measurements of the physical phantom, the mean wall thickness (±standard deviation)

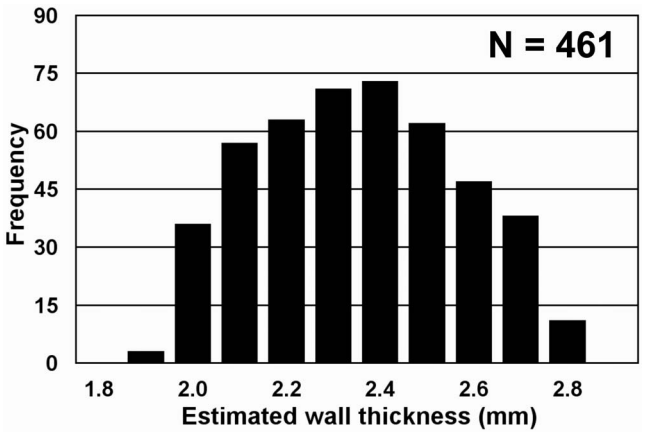

FIG. 5. A histogram shows the distribution of wall thickness using the three-dimensional, patch-by-patch approach on the surface sampled from the CT images of the physical phantom. Among 461 surface patches, the average wall thickness (±intra-measurement standard deviation) was 2.30 ± 0.21 mm, with the range from 1.9 to 2.7 mm.

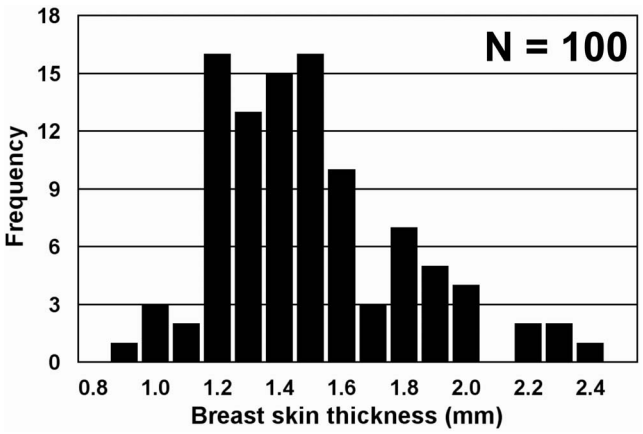

FIG. 6. A histogram showing the distribution of breast skin thickness using the three-dimensional, patch-by-patch approach on the breast surface sampled from the clinical bCT volumes. Among 100 breasts (51 women), the average breast skin thickness (±inter-breast standard deviation) was 1.45 ± 0.30 mm, ranged from 0.9 to 2.3 mm.

was 2.58 ± 0.17 mm. This measurement was considered as the truth to validate the accuracy of the algorithm. From the CT images of the physical phantom, the mean algorithm-measured thickness was 2.30 ± 0.21 mm. Although the estimated thickness was significantly different from the truth by approximately 0.2 mm ($p < 0.001$, Mann–Whitney rank sum test), the range of the truth thickness overlapped largely with that of the algorithm-measured thickness. Figure 5 illustrates the distribution of the estimated wall thickness of the physical phantom using 461 surface patches. The histogram displays a fairly concentrated profile close to the estimated wall thickness. This assessment suggests that the skin-thickness algorithm is accurate to within approximately 200 μm. Thus, the algorithm can be adapted to the clinical bCT data with the same degree of accuracy.

III.C. Skin thickness assessment

A histogram of breast skin thickness estimated by the 3D skin thickness algorithm among the entire patient population is shown in Fig. 6. Among 51 women, the mean breast skin thickness (±inter-breast standard deviation) was found to be 1.45 ± 0.30 mm (ranging from 0.9 to 2.3 mm). The mean breast skin thickness among the cancer-free breasts was found to be 1.45 ± 0.29 mm (ranged from 1.0 to 2.2 mm), while the average skin thickness among those with benign findings was 1.53 ± 0.54 mm (ranged from 1.2 to 1.9 mm). The mean skin thickness among breasts with biopsy-confirmed breast cancer was found to be 1.46 ± 0.32 mm (ranged from 0.9 to 2.3 mm). There was no significant difference between these three groups: benign versus cancer-free ($p = 0.918$, Mann–Whitney rank sum test), cancer-free versus breast cancer ($p = 0.712$, t test), and benign versus breast cancer ($p = 0.769$, t test). Among the three populations, most women (i.e., the 50% range) have breast skin thickness spanning between 1.2 and 1.6 mm.

The histogram of the breast skin thickness estimated from the 3D approach of one single breast was shown in Fig. 7. The skin thickness measurements from 692 breast surface patches demonstrated good precision with a mean skin thickness of 1.51 mm. Thus, the 3D surface fitting approach demonstrates the potential in reducing the bias from the non-normal crossing at the skin line.

The skin thickness was determined as a function of the anterior-posterior position in the breast. Figure 8 shows the skin thickness as a function of relative position (in percent) between the most posterior slice and the most anterior slice of the bCT volume set, for a representative woman in each of five bra cup size categories (A, B, C, D, and DD). Each breast image data set used in Fig. 8 represented the median breast volume for each bra cup size. Additionally, Table I lists the skin thickness distributions in Fig. 8 numerically to better demonstrate the intra-breast standard deviation due to the algorithm. The breast skin profiles along the breast length of five different women show fairly uniform skin thickness

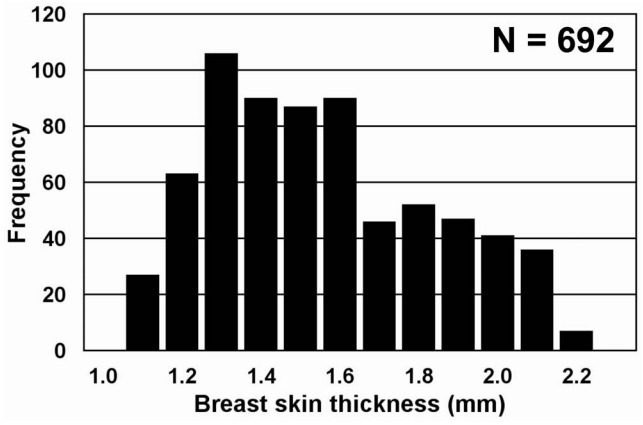

FIG. 7. A histogram of breast skin thickness using the three-dimensional surface-fit approach with one single bCT volume data set. Among the skin thickness measured from 692 breast surface patches, the mean skin thickness (±intra-breast standard deviation) was 1.51 ± 0.28 mm, with a range of 1.1–2.1 mm.

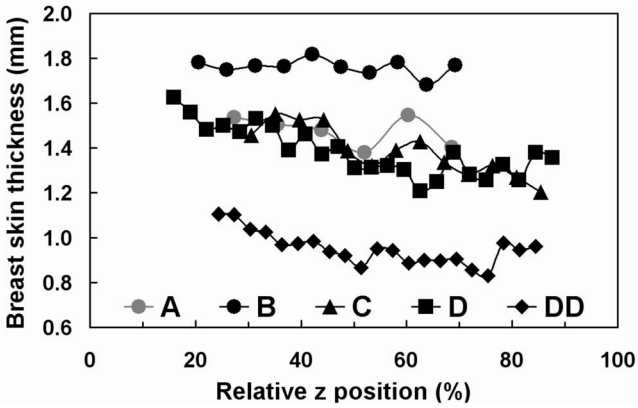

FIG. 8. The breast skin thickness as a function of anterior-posterior position in breasts of 5 women representative of each bra cup size category (A, B, C, D, and DD). The graph illustrates the profile of skin thickness along the anterior-posterior direction of each breast.

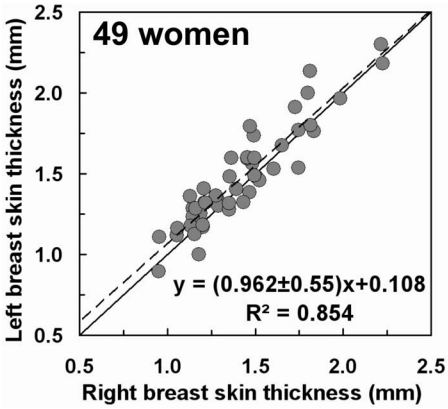

FIG. 9. The relationship between the right breast skin thickness and the left breast skin thickness of the same woman (49 women is shown; two women had data for only one breast). The solid line is the line of identity. The fitted slope is significantly different from 1.0 ($p=0.003$, paired t test).

across the entire breast surface. The fairly nonfluctuating trend seen in the profiles demonstrated the effectiveness of the 3D surface fitting approach to accurately measure the breast skin thickness at any 3D location on a breast skin surface.

Figure 9 shows the skin thickness of the left breast as a function of the skin thickness of the same woman's right breast. Linear regression was used to fit the left versus right breast skin thickness. The linear regression equation suggests that left breast skin thickness correlates with right breast skin thickness (slope ± slope variation of 0.96 ± 0.55, $r^2=0.8542$), as expected. Among 49 women, slightly thicker skin was observed in the left breast ($p=0.003$, paired t test). The thicker skin thickness in the left breast is likely due to the fact that left breasts were found to be slightly larger than right breasts in women.[14,15] The figure indicates some degree of uniform skin thickness between both breasts of a woman, which is an expected observation since skin thickness does not generally fluctuate largely over the both breasts.[16]

III.D. Breast dosimetry in mammography with Monte Carlo simulation

The Monte Carlo results of the normalized glandular dose (D_{gN}) coefficients for 4-cm and 6-cm 50% glandular breasts with different skin thickness (1.0–4.0 mm) are illustrated in Fig. 10. The curves show the D_{gN} values expressed in mean glandular dose per incident air kerma ($mGy \cdot mGy^{-1}$) over a range of x-ray spectra. Figure 11 demonstrates the influence of breast skin thickness in terms of the percentage increase in D_{gN} values relative to the assumption of a 4-mm skin thickness. Averaged over different x-ray spectra (24–35 kVp), D_{gN} values of a 4-cm 50% glandular breast increase by

TABLE I. A list of mean breast skin thickness (±intra-breast standard deviation) and the corresponding range for five different breasts (bra cup size A, B, C, D, and DD). The data represent the same volume sets whose profile distributions were shown in Fig. 8.

Bra cup size	Number of slice positions per breast volume set	Mean breast skin thickness ± intra-breast standard deviation (mm)	Breast skin thickness range (mm)
A	6	1.47 ± 0.07	1.4–1.5
B	10	1.76 ± 0.04	1.7–1.8
C	13	1.38 ± 0.10	1.2–1.6
D	24	1.38 ± 0.10	1.2–1.6
DD	21	0.95 ± 0.07	0.8–1.1

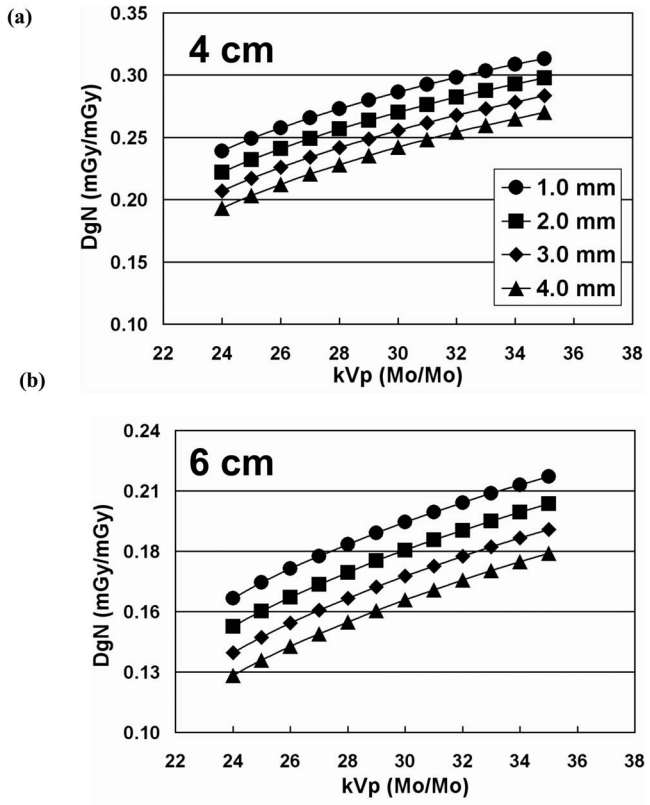

FIG. 10. The normalized glandular dose (D_{gN}) coefficients as a function of kVp for (a) a 4-cm 50% glandular breast and (b) a 6-cm 50% glandular breast with 1.0-, 2.0-, 3.0-, and 4.0-mm skin thickness.

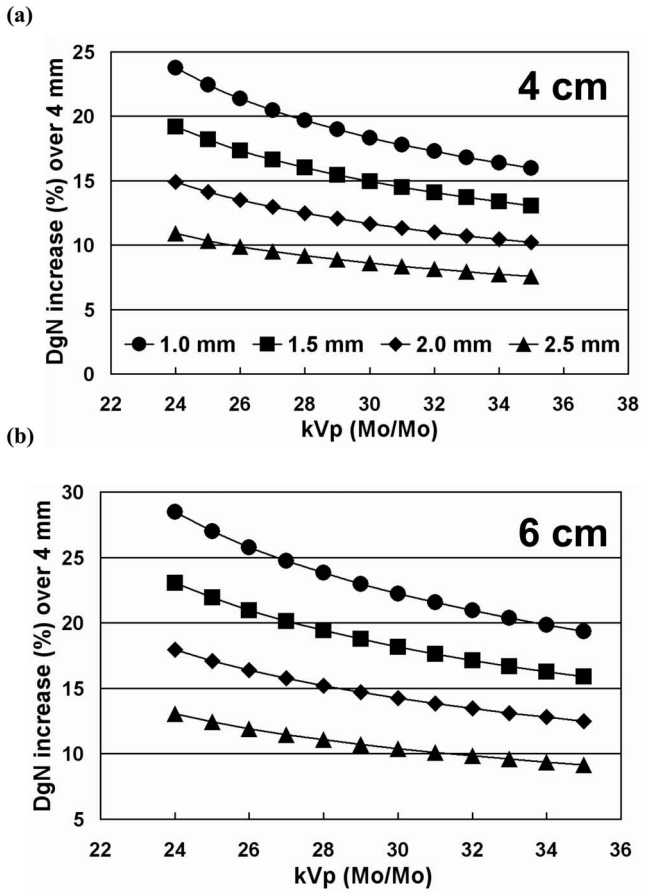

FIG. 11. The D_{gN} increase (%) over that of a breast with 4-mm skin thickness as a function of kVp for (a) a 4-cm 50% glandular breast and (b) a 6-cm 50% glandular breast with 1.0-, 1.5-, 2.0-, and 2.5-mm skin thickness.

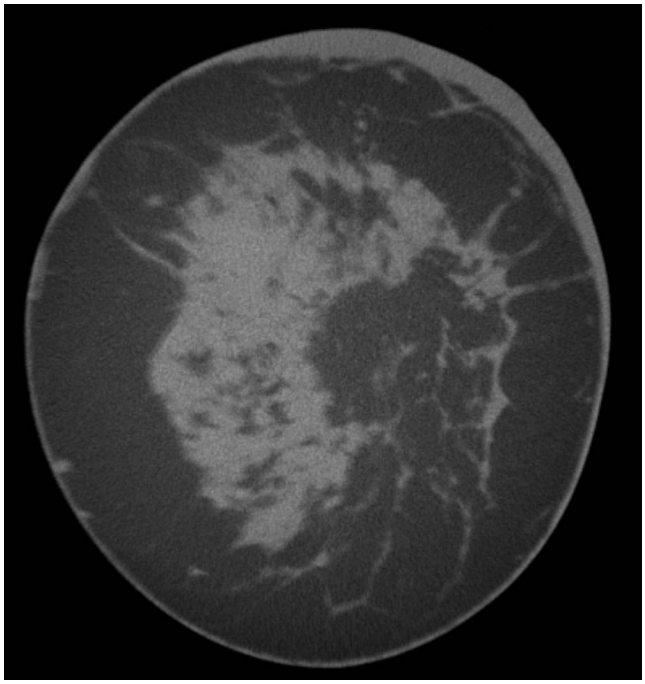

FIG. 12. A coronal bCT image of a recent bCT participant displays local skin thickening in the breast with biopsy-confirmed breast cancer.

9.0% ± 1.1% (standard deviation) for a 2.5-mm skin thickness and by 16.0% ± 2.0% for a 1.5-mm skin thickness. For a 6-cm 50% glandular breast, the D_{gN} values increase on average by 11.0% ± 1.3% for a 2.5-mm skin thickness and by 19.0% ± 2.3% for a 1.5-mm skin thickness.

IV. DISCUSSION

A comprehensive evaluation of breast skin thickness was performed across breast CT image data sets from 51 women. In the early era of screen-film mammography, the thickness of the normal skin was widely quoted to be in the range from 0.5 to 1.5 mm.[16] In more recent studies, the normal skin thickness of the breast was found to be slightly thicker, ranging from 0.7 to 3.0 mm.[17,18] Another recent study found that mammographic skin thickness ranged from 0.5 to 3.1 mm.[19] Our study has found a similar skin range (1.0–2.2 mm) among cancer-free breasts compared to the skin thickness range determined in previous studies.

Skin thickness is one of the parameters considered in assessing the radiation dose in mammography. The skin thickness was assumed to be 4–5 mm for most Monte Carlo based studies of D_{gN} values performed in the past.[3–8] The smaller average skin thickness (1.45 mm) found in this study will result in slightly higher D_{gN} coefficients than those computed using greater skin thicknesses in the Monte Carlo computations. Figures 10 and 11 demonstrate that a non-negligible increase in D_{gN} values occurs for typical mammographic spectra (24–35 kVp) when a thinner skin layer was used.

Normal human skin is comprised of three main layers: the epidermis, dermis, and subcutaneous fat tissues. The epidermis layer has a quoted range between 0.07 and 1.4 mm and the dermis layer is quoted to range between 0.6 and 3.0 mm.[20] The average skin depth, including only the epidermis and dermis layers, was quoted to be 2.54 mm.[20] If indeed the subcutaneous fat layer of the skin (which is probably not resolved with breast CT) is distinct and isolated from the adipose tissue of the breast parenchyma, the thicker skin layer would act to shield the breast and existing D_{gN} values would likely to be accurate. If, however, glandular tissue filaments (which is the tissue at risk for breast cancer) can extend into the subcutaneous fat layer as anecdotal evidence from the breast CT images suggests, the thinner skin layers would imply that a slight increase in D_{gN} values would be warranted.

Although our study has shown that there is no significant difference among the skin thickness of three breast populations (cancer-free, benign, and cancer), Fig. 12 demonstrates local skin thickening in a recent bCT data of a woman with biopsy-confirmed breast cancer. Previous studies have shown the prognostic significance of the mammographically demonstrated skin thickening among noninflammatory breast cancer.[21,22] However, the correlation between breast cancer development and skin thickening is out of the scope of this study.

V. CONCLUSIONS

Breast CT images were used to assess skin thickness using an automated algorithm. The algorithm's accuracy was assessed against physical measurements of a breast-shaped phantom and found to be within 0.20 mm. The overall breast skin thickness from the 51 women assessed in this study was found to average 1.45 mm $\pm$ 0.30 mm. Most Monte Carlo derived dose conversion coefficients (D_{gN} coefficients) used for dosimetry in mammography assume a 4.0-mm breast skin thickness, and the thinner skin thickness found in this study would imply that a slight increase of 10%–20% in D_{gN} coefficients may be warranted.

ACKNOWLEDGMENTS

This research was funded in part from California Breast Cancer Research Program (Grant No. 11IB-0114), the National Institute for Biomedical Imaging and Bioengineering (Grant No. EB002138-03), National Cancer Institute (Grant No. CA-89260), and the Susan G. Komen Foundation (Grant No. BCTR0503516). The machine shop affiliated with Professor Neville C. Luhmann (The Millimeter Wave Group, Department of Applied Science, University of California, Davis) was most helpful in the measurement of the physical phantom. The technical guidance from this group is gratefully acknowledged.

[a]Electronic mail: jmboone@ucdavis.edu

[1]J. M. Boone, M. H. Buonocore, and V. N. Cooper, "Monte Carlo validation in diagnostic radiological imaging," Med. Phys. **27**, 1294 (2000).
[2]J. M. Boone and V. N. Cooper III, "Scatter/primary in mammography: Monte Carlo validation," Med. Phys. **27**, 1818–1831 (2000).
[3]M. Rosenstein, L. W. Andersen, and G. B. Warner, *Handbook of Glandular Tissue Doses in Mammography* (U.S. Dept. of Health and Human Services, Public Health Service, Food and Drug Administration, Center for Devices and Radiological Health, Rockville, MD, 1985).
[4]D. R. Dance, "The Monte Carlo calculation of integral radiation dose in xeromammography," Phys. Med. Biol. **25**, 25–37 (1980).
[5]X. Wu, E. L. Gingold, G. T. Barnes, and D. M. Tucker, "Normalized average glandular dose in molybdenum target-rhodium filter and rhodium target-rhodium filter mammography," Radiology **193**, 83–89 (1994).
[6]D. R. Dance, "Monte Carlo calculation of conversion factors for the estimation of mean glandular breast dose," Phys. Med. Biol. **35**, 1211–1219 (1990).
[7]X. Wu, G. T. Barnes, and D. M. Tucker, "Spectral dependence of glandular tissue dose in screen-film mammography," Radiology **179**, 143–148 (1991).
[8]J. M. Boone, "Glandular breast dose for monoenergetic and high-energy X-ray beams: Monte Carlo assessment," Radiology **213**, 23–37 (1999).
[9]J. M. Boone, A. L. Kwan, J. A. Seibert, N. Shah, K. K. Lindfors, and T. R. Nelson, "Technique factors and their relationship to radiation dose in pendant geometry breast CT," Med. Phys. **32**, 3767–3776 (2005).
[10]K. Yang, A. Kwan, G. Burkett, and J. M. Boone, "Hounsfield units calibration with adaptive compensation of beam hardening for a dose limited breast CT system (abstract)," American Association of Physicists in Medicine 28th Annual Meeting, Orlando, Florida, July 30–August 3, 2006 (unpublished).
[11]K. Yang, A. L. Kwan, D. F. Miller, and J. M. Boone, "A geometric calibration method for cone beam CT systems," Med. Phys. **33**, 1695–1706 (2006).
[12]C. R. Gonzalez and R. E. Woods, *Digital Image Processing*, 2nd ed. (Prentice Hall, Upper Saddle River, NJ, 2002).
[13]http://www.csse.uwa.edu.au/~pk/research/matlabfns/.
[14]J. T. Manning, D. Scutt, G. H. Whitehouse, and S. J. Leinster, "Breast asymmetry and phenotypic quality in women," Evol. Hum. Behav. **18**, 223–236 (1997).
[15]D. Scutt, G. A. Lancaster, and J. T. Manning, "Breast asymmetry and predisposition to breast cancer," Breast Cancer Res. **8**, R14 (2006).
[16]D. M. Witten, *The Breast* (Year Book Medical, Chicago, 1969), p. 15.
[17]T. L. Pope, Jr., M. E. Read, T. Medsker, A. J. Buschi, and A. N. Brenbridge, "Breast skin thickness: Normal range and causes of thickening shown on film-screen mammography," J. Can. Assoc. Radiol. **35**, 365–368 (1984).
[18]S. A. Willson, E. J. Adam, and A. K. Tucker, "Patterns of breast skin thickness in normal mammograms," Clin. Radiol. **33**, 691–693 (1982).
[19]H. Ulger, N. Erdogan, S. Kumanlioglu, and E. Unur, "Effect of age, breast size, menopausal and hormonal status on mammographic skin thickness," Skin Res. Technol. **9**, 284–289 (2003).
[20]http://www.pride.hofstra.edu/~BCIAVA1/BURNS.HTM.
[21]H. S. Shukla, L. E. Hughes, I. H. Gravelle, and A. Satir, "The significance of mammary skin edema in noninflammatory breast cancer," Ann. Surg. **189**, 53–57 (1979).
[22]H. S. Shukla, I. H. Gravelle, L. E. Hughes, R. G. Newcombe, and S. Williams, "Mammary skin oedema: A new prognostic indicator for breast cancer," Br. Med. J. (Clin. Res. Ed.) **288**, 1338–1341 (1984).